applied sciences

MDPI

Article

Lifetime Assessment and Optimization of a Welded A-Type Frame in a Mining Truck Considering Uncertainties of Material Properties and Structural Geometry and Load

Chengji Mi [1,2], Wentai Li [1], Xuewen Xiao [1], Haigen Jian [1,*], Zhengqi Gu [1,2] and Filippo Berto [3]

[1] Hunan University of Technology, Zhuzhou 412007, China; michengji_86@126.com (C.M.); liwentai2019@126.com (W.L.); 13838@hut.edu.cn (X.X.); guzhengqi63@126.com (Z.G.)
[2] State Key Laboratory of Advanced Design and Manufacturing for Vehicle Body, Hunan University, Changsha 410082, Hunan, China
[3] Norwegian University of Science and Technology, 7491 Trondheim, Norway; filippo.berto@ntnu.no
* Correspondence: jianhaigen2001@163.com

Received: 19 December 2018; Accepted: 26 February 2019; Published: 4 March 2019

Abstract: In order to improve the fatigue performance of a welded A-type frame in a heavy off-road mining truck, a novel method was presented to implement lifetime and weight collaborative optimization while considering uncertainties in geometry dimension, material properties, and bearing load. The mechanical and cyclic material parameters were obtained from experimental work to characterize the base metal and the weldment. The finite element model of a welded A-type frame was constructed to analyze stress distribution and predict fatigue life, the force time histories of which were acquired from multi-body dynamics simulation. The simulated failure position and fatigue life had a good agreement with the actual results. Then, both structural lifetime and weight were considered as optimization objectives. The thickness of main steel plates and elastic and cyclic material parameters were chosen as uncertain design variables as well as main loads at connection locations. The fifty sample points in the light of Latin hypercube sampling method and its responses calculated by finite element analysis were supposed to build the approximation model based on the Kriging approximation method. After its fitting precision was guaranteed, the non-dominated sorting genetic algorithm II (NSGA-II) was utilized to find the optimal solution. Finally, the fatigue life of a welded A-type frame was increased to 2.40×10^5 cycles and its mass was lessened by 8.2%. The optimized results implied that good fatigue performance of this welded A-type frame needs better welding quality, lower running speed for downhill and turning road surface, and thicker front plates.

Keywords: welded structure; fatigue characterization; multi-source uncertainty; multi-objectives optimization; Kriging approximation method

1. Introduction

The welded A-type frame of steering system is considered as one main bearing component for mining dump trucks. Its fatigue performance is seriously concerned when the truck runs on poor road surface with hundreds of tons of goods. This frame is welded with different thickness of plates; however, fatigue cracks often start from weld toe located at stress concentration areas [1].

There are several methods to predict fatigue life of a welded structure. These could be categorized into nominal stress [2,3], structural stress [4], local notch [5], and fracture mechanics approaches [6]. The fracture mechanics method firstly assumes that the crack or crack-like flaw exists in the weld metal,

and the stress intensity factor or J-integral is considered as the fatigue damage parameter, related with lifetime or crack growth rate [7]. The local notch approach is defined by using local stress, local strain, or local energy at the notch tip to estimate fatigue strength. The advantage of this method is that the effect of notch characteristics and cyclic material properties could both be included [8,9]. The structural stress method focuses on a linearly distributed stress along the thickness without considering the stress concentration. Superposing the mechanical responses caused by forces and moments, the linear elastic finite element analysis is often implemented to calculate structural stress and strain, which is coupled into the mathematical model to assess fatigue life [10]. The nominal stress amplitude in the critical cross-section is treated as a fatigue damage parameter without consideration of the stress concentration at the weld toe and dissimilar material properties. This method is based on the S-N curve and preferred in many engineering areas because of its simplicity, such as in vehicles, vessels, and bridges [11]. According to those rules, Shao et al. [12] estimate lifetime of drive axle housing for a mining truck by measuring strains at hot spots, which were transformed to stress spectrum. Then, the stress amplitude and stress mean with their cycles were counted using the Rain-flow method, and Morrow's stress-life equation was utilized to obtain the service lives. Mi et al. [13,14] conducted a fatigue life assessment of the frame by combining multi-body dynamics analysis with finite element analysis to acquire the stress and strain spectrum. The service life was calculated as Palmgren-Miner's linear damage accumulation rule and normal S-N curve. In order to exactly present fatigue life distribution for a welded mining truck's frame at critical areas, even the total strain energy density was used as a fatigue damage parameter to predict lifetime, based on fitting the relationship between fatigue life and elastic and plastic strain energy density [15]. Moreover, the local strain energy density averaged over the control volume surrounding the crack tip in the weakest point of the roller was supposed to characterize the fatigue strength of welded joints [16,17].

When the actual fatigue life or predicted lifetime of engineering structures is less than the required one, the fatigue optimization design is indispensable. In order to simultaneously enhance the performance and robustness of the fatigue life for a truck cab, Fang et al. [18] present a dual Kriging surrogate modeling method to overcome the limitation of classical dual response surface method. The reliability-based design optimization is proposed by the Aoues et al. [19,20] and aims to find the most balanced design through a compromise between cost and safety when uncertainties affect the system. Moreover, Gao et al. [21] constructed a lightweight optimization model with static strength and weld fatigue constraints for the welded frame of a three-axle bogie, which is solved by an adaptive sequential approximation optimization method based on Kriging models.

Most of optimization procedures mentioned above predominately focus on the single optimization objective, such as minimizing structural weight or maximizing lifetime. Sometimes the re-optimization design is needed in the presence of contradictory results between different required performances. In the meanwhile, the variables for the general optimization design only depend on the structural dimensions or process parameters, while the material properties or loads are deemed to be the deterministic values. However, the material parameters are related with artificial manufacturing procedures, and they should be random due to uncertain technological conditions, as well as loads in the utilizations. Therefore, this paper presents a fatigue life and weight co-optimization method to obtain the compatible optimal results for a welded A-type frame in a mining dump truck. Moreover, it considers that there are some deviations in structural geometry in the design stage, and material properties are also varied under different manufacturing processes, as well as loads in different usage conditions. The multi-source uncertainty variables including structural geometry dimensions, material properties, and loads were all considered when conducting multi-objective optimization design in this paper.

Then, the monotonic tensile and fatigue tests of welded joints were studied to obtain the mechanical material parameters for the both base metal and weld metal and cyclic properties for the weld metal. The strain-life curve was considered as the calculation basis in the following lifetime prediction. The micro properties were also observed to understand the fatigue characteristics of this

weld metal. A multi-body dynamic model was built to obtain the load history and its accuracy was verified by comparing the simulated results with the experimental ones. The finite element model of welded A-type frame was also constructed and validated. The elastic and plastic finite element analysis of this frame was performed and its fatigue life was calculated as per the Manson-Coffin equation. The multi-objective optimization function was built by considering the multi-source uncertainties in different stages. The 50 sample points were obtained from the Latin hypercube sampling method. Based on the Kriging approximation model, the optimization mathematical model was constructed and validated by 10 other sample points. To obtain the optimal result, the NSGA-II was utilized to determine the Pareto solution sets.

2. Cracks in Local Positions

This truck equipped with more than 200 tons of minerals usually runs on the downhill and turning road surface at the speed of 35 km/h, shown in Figure 1. As main load-bearing part, the welded A-type frame in steering system of heavy off-road mining truck has to withstand huge force from connection joints in this case. However, the stress concentration is usually generated in structural weakness regions, especially in geometric transition. The crack then appears along the weld toe under cyclic loads for some trucks, seen in Figure 2. The fatigue performance of this frame is one of critical factors to ensure truck's running reliability and safety. Therefore, anti-fatigue optimization design for the welded A-type frame is conducted to improve its service lifetime.

Figure 1. Practical mine pavement.

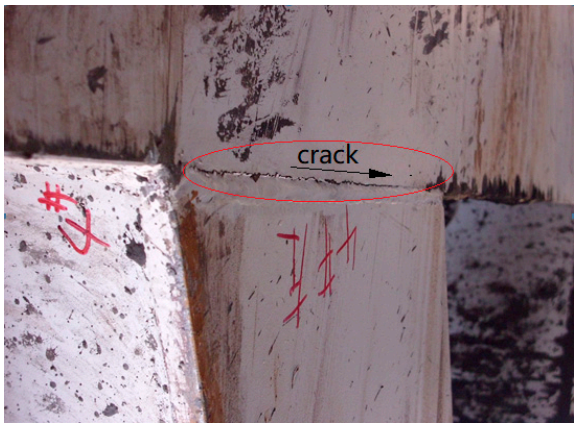

Figure 2. Crack in welded A-type frame.

3. Experimental Work

3.1. Specimen and Elements

The material used in this frame is one kind of high strength low alloy steel under quenched and tempered conditions. The elements of both base metal and the weld seam were listed in Table 1.

Table 1. Chemical elements of base metal and weldment (%).

Material	Fe	Mn	S	Cr	Ni	Si	Ti	C
Base metal	96.19	2.11	0.30	0.25	0.30	0.46	0.19	Bal.
Weldment	96.15	1.61	0.18	0.39	0.62	0.89	0.05	Bal.

The geometry dimension of specimen was designed like a flat dog-bone; its thickness was 2.5 mm and 6 mm for the base metal and the weldment, respectively, as shown in Figure 3. This butt joint processed by gas metal arc-welding was used to obtain the welded frame's material characteristics.

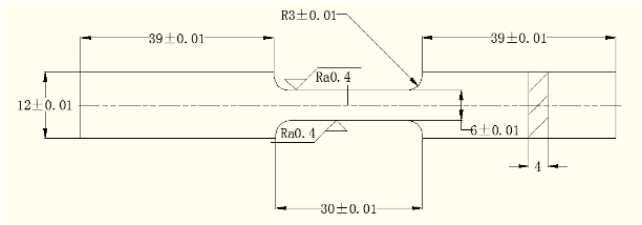

(**a**)

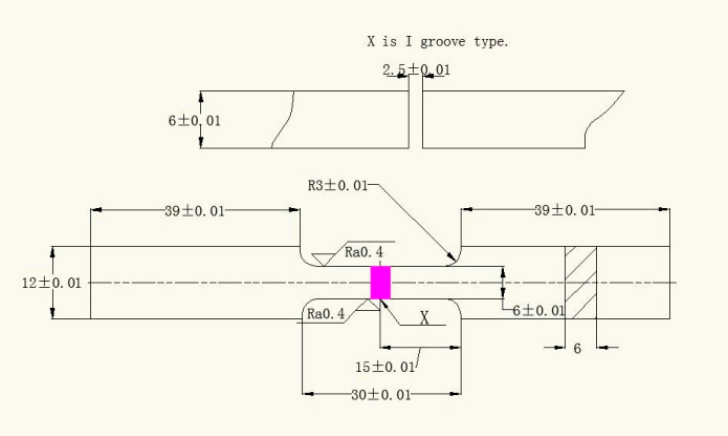

(**b**)

Figure 3. Specimen geometry dimension: (**a**) base metal; (**b**) weldment; (all dimensions in mm, roughness in micro meters).

3.2. Mechanical Properties

The installation diagram of monotonic tensile test is shown in Figure 4. The monotonic tensile tests were conducted on both base metal and weldment specimens at the rate of 0.025 mm/sec, at normal room temperature and humidity. Both engineering and actual stress/strain curves for the base metal and the weld metal are shown in Figures 4 and 5. The mechanical properties under monotonic tensile tests are listed in Table 2. Their standard deviations signified that the repeatability of the tests was acceptable. It was clearly seen that the yield strength of the base metal was close to the weld metal and their difference of ultimate tensile strength (UTS) was also small.

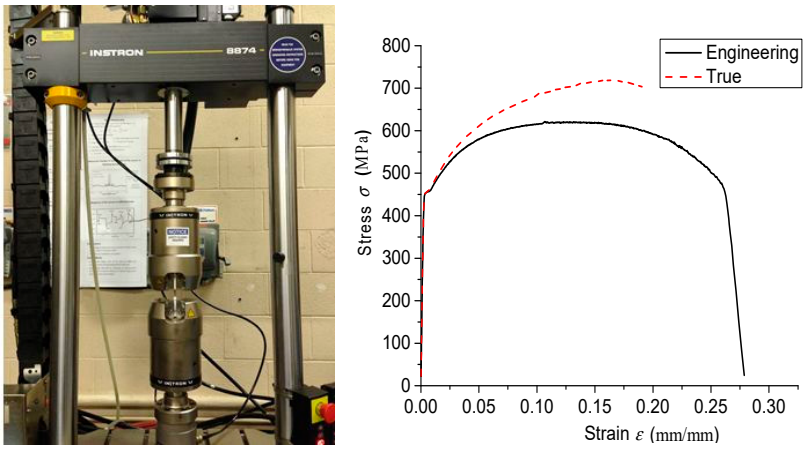

(**a**) (**b**)

Figure 4. (**a**) Installation diagram of monotonic tensile test; (**b**) Stress and strain curve of base metal under monotonic tensile test.

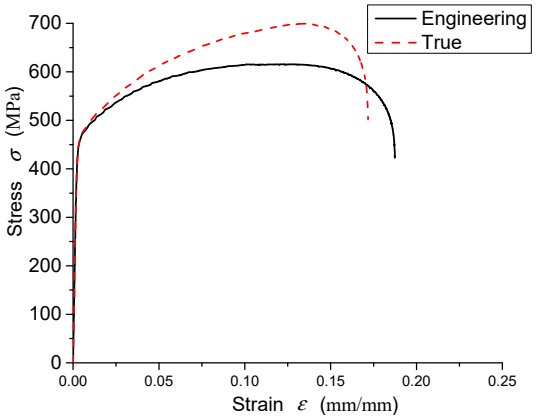

Figure 5. Stress and strain curve of weldment under monotonic tensile test.

Table 2. Mechanical properties under monotonic tensile test.

	Base Metal	**Weldment**
Young's modulus E (GPa)	200.4	210.1
Yield Strength σ_s (MPa)	451	456
UTS σ_b (MPa)	621.5	615.9
Elongation e_f (%)	27	18
True fracture stress σ_t (MPa)	57	24
True fracture strain e_t (%)	0.336	0.279

3.3. Cyclic Properties of a Welded Joint

The crack initiation of welded A-type frame started from the weld toe, as shown in Figure 2, so it was necessary to figure out the cyclic characteristics of the weld metal. Fully reversed cyclic loading was applied on the flat butt joint under strain control, and the strain amplitude changed from 0.1% to 0.45%. The gage length of the extensometer was 10 mm. The fatigue failure criterion was 50% drop of load. The strain was measured by an Epsilon uniaxial extensometer to obtain cyclic mechanical responses. For the low strain amplitude testing, the 70 MPa cyclic loading under load control was first performed on the specimen for 0.1 million cycles to make the weld metal stable and avoid a possible buckling phenomenon. For the high strain amplitude testing, the low loading frequency with no more than 1 Hz was required to keep the material stable. The experimental results between all strain amplitudes and number of reversals ($2N$) are shown in Figure 6.

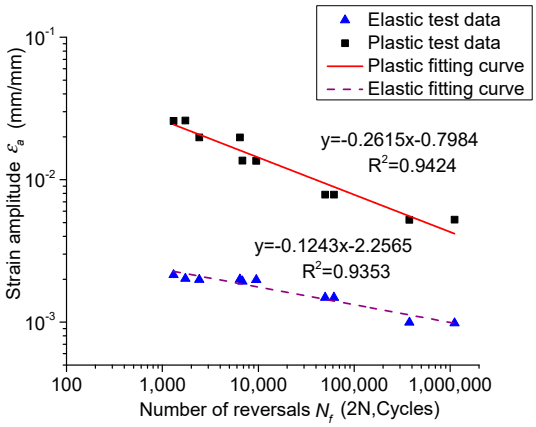

Figure 6. Relationship between strain amplitude and cycles under cyclic loading.

In order to acquire cyclic properties, the Manson-Coffin equation was utilized to describe the fatigue characteristics:

$$\varepsilon_a = \frac{\Delta\varepsilon^e}{2} + \frac{\Delta\varepsilon^p}{2} = \frac{\sigma_f'}{E}(2N_f)^b + \varepsilon_f'(2N_f)^c \quad (1)$$

where ε_a is total strain amplitude, and $\Delta\varepsilon^e/2$ and $\Delta\varepsilon^p/2$ are elastic and plastic strain amplitude, respectively. The fatigue strength coefficient and the fatigue ductility coefficient are represented by σ_f' and ε_f', respectively. The fatigue strength exponent and the fatigue ductility exponent are represented by b and c, respectively.

The cyclic stress versus strain relationship for the weld metal could be described by the Ramberg-Osgood equation as:

$$\varepsilon_a = \frac{\Delta\sigma/2}{E} + \left(\frac{\Delta\sigma/2}{K'}\right)^{1/n'} \quad (2)$$

where $\Delta\sigma/2$ is the stabilized stress amplitude, and K' is the cyclic strength coefficient, and n' is the cyclic strain hardening exponent, respectively. The Ramberg-Osgood coefficients were calculated by fitting a curve with power equation to experimental plastic strain amplitude and stress, as shown in Figure 7. Those parameters are listed in Table 3.

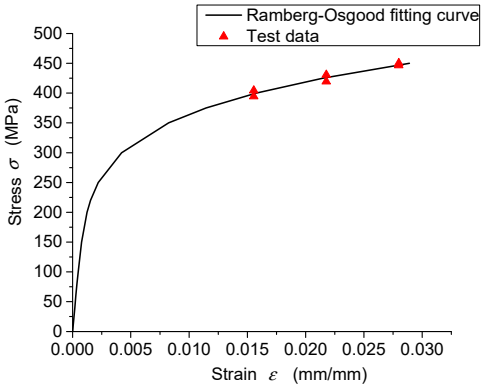

Figure 7. Fitting curve for Ramberg-Osgood coefficients.

Table 3. Fatigue parameters of the welded joint.

σ_f' (MPa)	b	ε_f'	c	K'	n'
1163.4	−0.1243	0.159	−0.2615	860.99	0.1792

To clarify the material parameters mentioned above, the total strain amplitude was decomposed to elastic and plastic parts, as shown in Figure 6. Then, the cyclic parameters were calculated by fitting linear curves under logarithmic coordinate to be elastic and plastic strain amplitude versus number of reversals. Those parameters are listed in Table 3. According to the results, the plastic strain amplitude was much higher than the elastic strain amplitude for each strain level. The fitting curve could perfectly describe the cyclic response, as displayed in Figure 8. According to cyclic stress and strain relationship shown in Figure 9, the second cycle stress at 0.25% strain level was much higher than the half cycle, which implied that this material has cyclic softening.

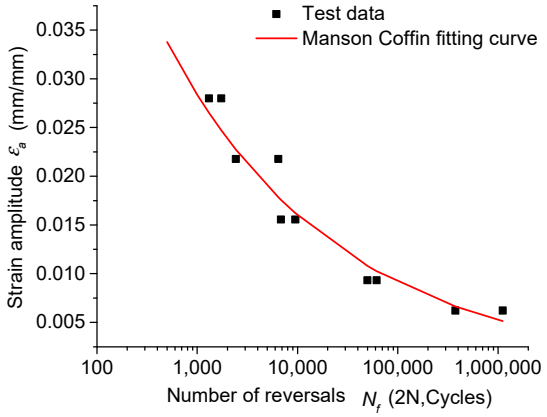

Figure 8. Manson-Coffin fitting curve.

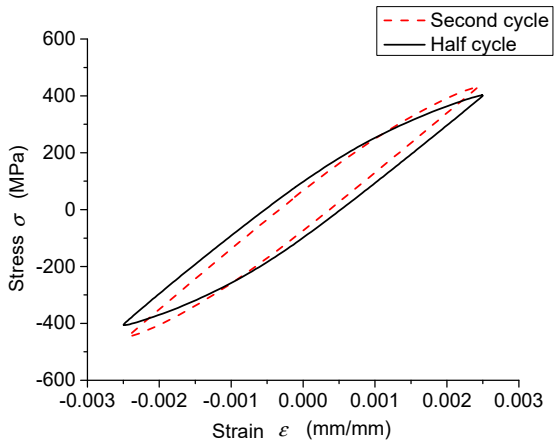

Figure 9. Cyclic strain and stress at 0.25% strain level.

3.4. Microscopic Properties

In order to gain a deeper understanding of the fatigue characteristics, the microstructure for the base metal and the weld seam were both observed by transmission electron microscope (TEM), as shown in Figures 10 and 11. The grain size at the base zone was small, fine equiaxed grain. The big grain located at the heat affected zone was stretched along the thermal gradient direction during the welding process to become middle equiaxed grain. The temperature inconsistency resulted in the local grain coarsening. In addition, for the high fatigue regime, the fracture site had wave strips and loads of tiny steps caused by secondary extrusion under high frequency load, displayed in Figure 12. For the low fatigue regime, there were persistent slip bands, extrusion spines, and ditches under high strain amplitude loading, which was formed by uneven slip around metal surface, displayed in Figure 13.

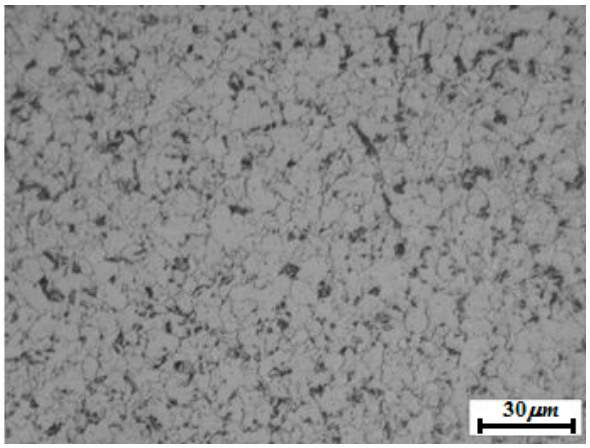

Figure 10. Microstructure at the base zone.

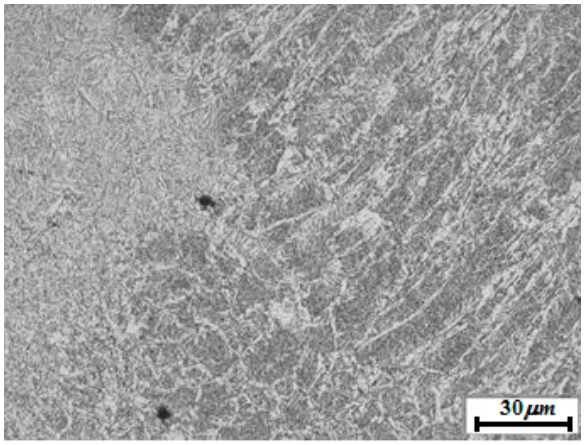

Figure 11. Microstructure at the heat affected zone.

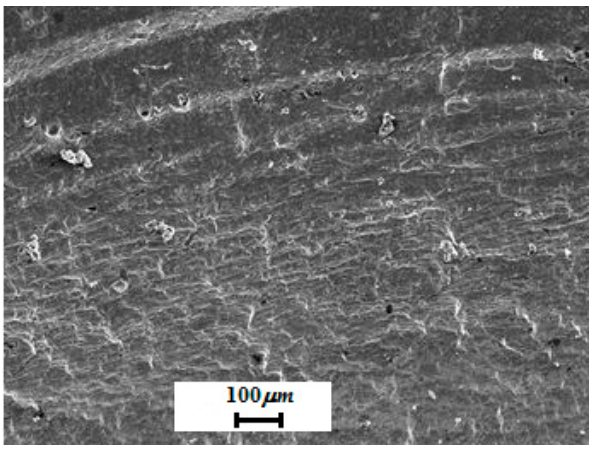

Figure 12. High-cycle fatigue fracture morphology.

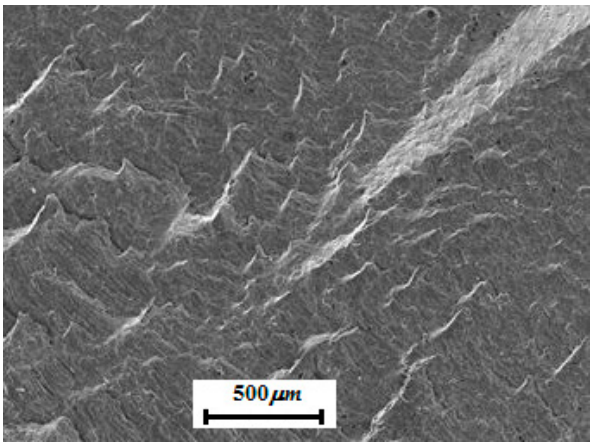

Figure 13. Low-cycle fatigue fracture morphology.

4. Fatigue Life Estimation

4.1. Multibody Dynamics Analysis

To obtain force load history needed in fatigue life estimation of welded A-type frame, a multi-body dynamic model for the whole vehicle was constructed using the ADAMS software for simulating real operating conditions. The truck model and the horizontal surface are shown in Figure 14. A complete description of this modeling can be found in Refs. [1,13,14]. To verify the accuracy of this multi-body dynamic model, the acceleration time history of wheel center at the speed 30 km/h obtained from the simulation was compared with the tested results, displayed in Figure 15. The acceleration time history and its frequency spectrum matched were well-matched between them. However, there were several peaks in the tested acceleration frequency spectrum around 30 Hz. It could be caused by the external interferences or operational errors. The differences of the root mean square acceleration for the wheel center at different speed between the test and simulation were small, as shown in Figure 16.

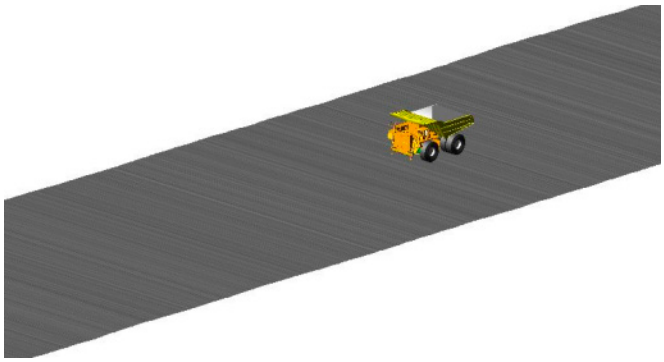

Figure 14. Multi-body dynamics model.

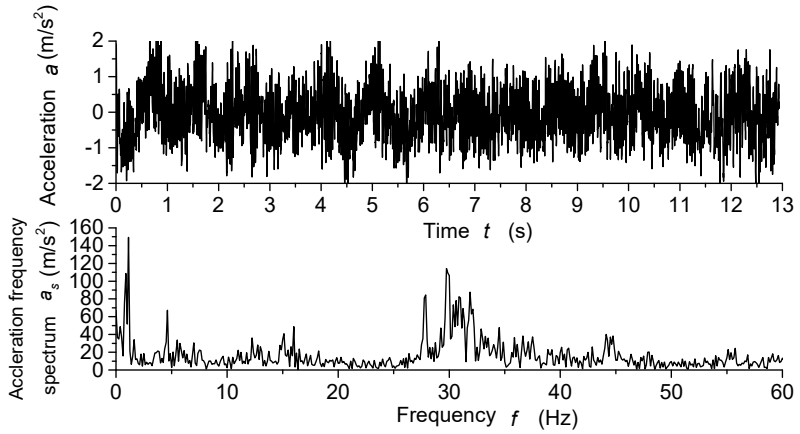

(**a**)

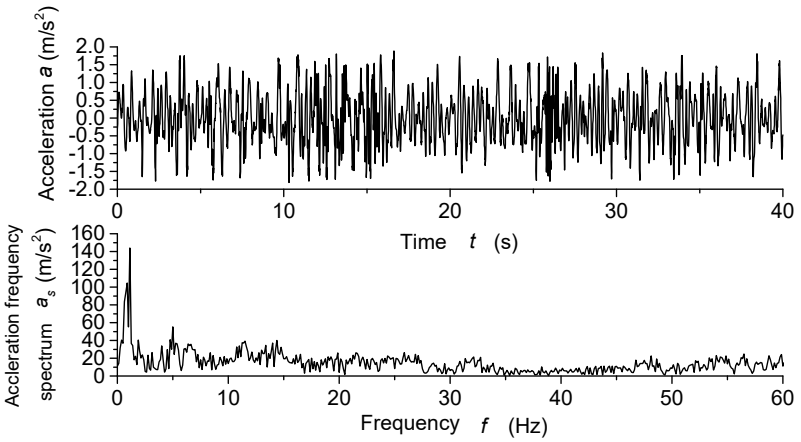

(**b**)

Figure 15. Acceleration time history and its frequency spectrum of wheel center at the speed 30 km/h: (**a**) tested results; (**b**) simulated results.

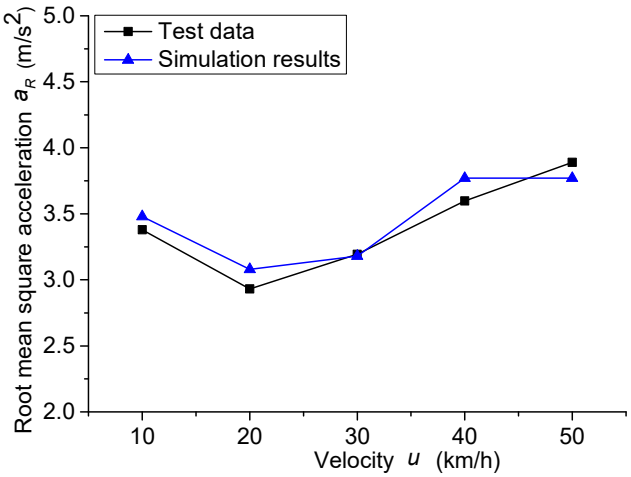

Figure 16. Root mean square acceleration of wheel center at different speed.

When the precision of multi-body dynamic model was guaranteed, the downhill and turning road surface was built to simulate bad working conditions. The starting speed of the truck was defined as 30 km/h, and the turning radius was 60 m, shown in Figure 17. The simulation time was 16.5 s. Then, the force time history of welded A-type frame at connection sites was acquired from multi-body

dynamics analysis, shown in Figure 18, which was considered as cyclic load required for fatigue life prediction.

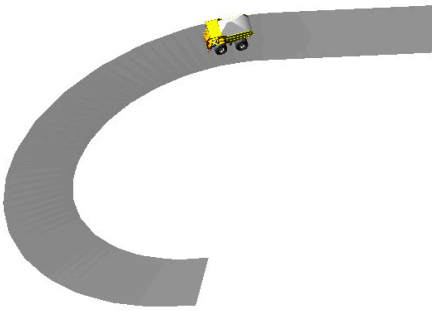

Figure 17. Multi-body dynamics model for downhill and turning condition.

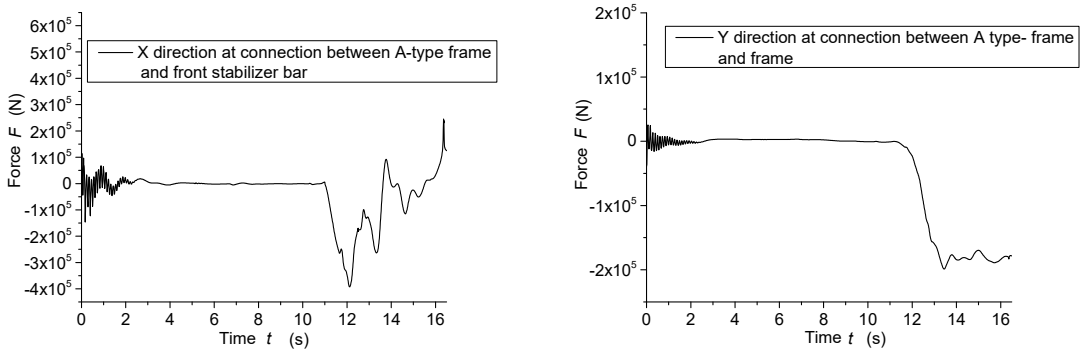

(**a**) (**b**)

Figure 18. Force time history of welded A-type frame: (**a**) connection site between A-type frame and front stabilizer bar; (**b**) connection site between A-type frame and frame.

4.2. Elastic/Plastic Analysis and Verification

The FE model of welded A-type frame was generated using HYPERMESH software to estimate the lifetime under its force time history. The frame structure made up of front plates and back plates was meshed with 83,648 solid elements, including 81,907 C3D8 and 1741 C3D6. The average length of the meshed elements was 2 mm. The cracked region of the weld seam was endowed with gradual meshing, as shown in Figure 19. The connection site between A-type frame and suspension (marked as A5 in Figure 19) was constrained with all degrees of freedom. The connection sites between A-type frame and frame (marked as A1 in Figure 19), right and left steering cylinder (marked as A3 and A2 in Figure 19), and front stabilizer bar (marked as A4 in Figure 19) were applied with the simulated force obtained from the multi-body dynamics analysis, respectively. The material properties for elastic/plastic finite element analysis were based on the cyclic characteristics, according to the parameters listed in Table 3. The Von-Mises stress contour of the welded A-type frame under the downhill and turning road surface condition is shown in Figure 20. The maximum stress was at the bottom corner between right front plate and back plate, which was close to the actual failure position. The critical regions at the bottom and top corner between front plate and back plate all had high stress levels as well.

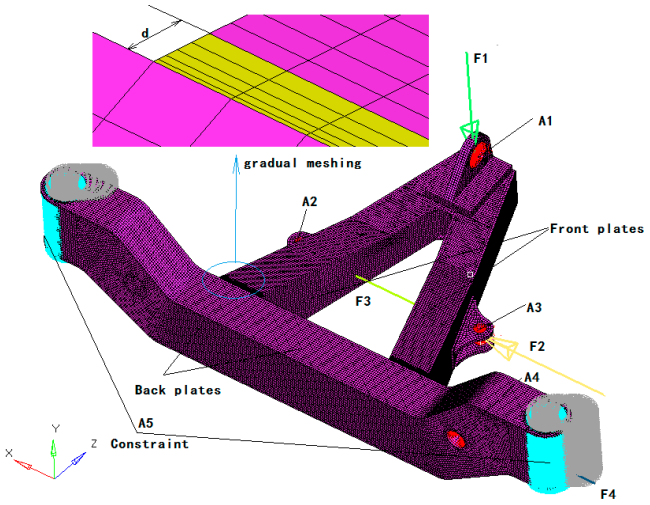

Figure 19. Finite element model of welded A-type frame.

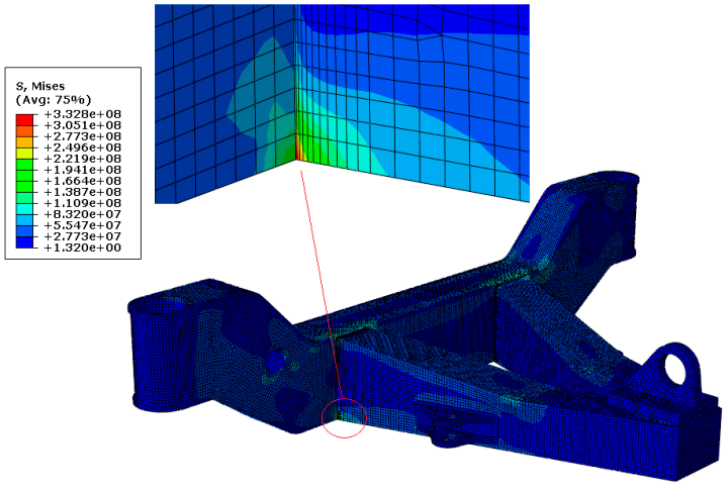

Figure 20. Von-Mises stress contour of welded A-type frame, units in Pa.

To verify the finite element model, the strain measurements were conducted by using strain gauge rosettes under the downhill and turning road surface condition. The measuring points were considered as potential high stress ones, shown in Figure 21; the local strain gauge layout at measuring point A1-2 is displayed in Figure 22. Then, the tested principal stresses were compared with the simulated results, which were calculated from the measured strain values as the following equation:

$$\sigma_{1,2} = \frac{E}{2(1-\mu)}(\varepsilon_{0^\circ} + \varepsilon_{90^\circ}) \pm \frac{E}{\sqrt{2}(1+\mu)} \cdot \sqrt{(\varepsilon_{0^\circ} - \varepsilon_{45^\circ})^2 + (\varepsilon_{45^\circ} - \varepsilon_{90^\circ})^2} \quad (3)$$

where $\sigma_{1,2}$ are the principal stress, E and μ are Yong's modulus and Poisson's ratio, and ε_{0°, ε_{45°, ε_{90° are the strain components along the three directions of the strain rosette.

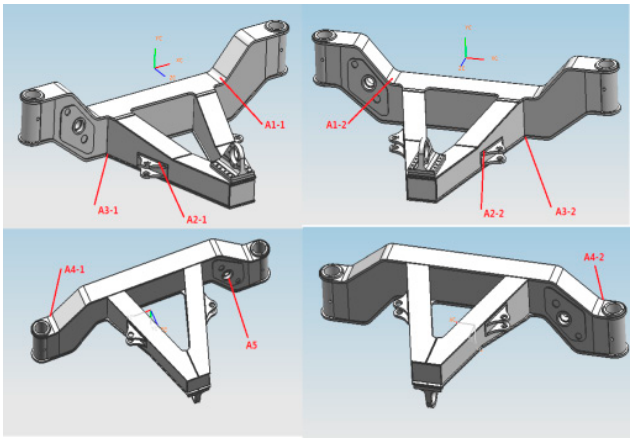

Figure 21. Schematic diagram of measuring points of welded A-type frame.

Figure 22. Layout of measuring point A1-2.

The simulated principal stresses could then be obtained from finite element analysis, which were compared with the experimental results, listed in Table 4. From the comparison, it was clearly seen that the finite element analysis results agreed well with the tested ones. Most of the relative errors were less than 10%, which is acceptable in engineering structure simulation.

Table 4. Comparison between simulated and tested principal stress (MPa).

	A1-1	A1-2	A2-1	A2-2	A3-1	A3-2	A4-1	A4-2	A5
Simulated stress	101	117	79	98	333	301	75	81	109
Tested stress	92	105	71	92	316	285	69	78	97
Error	9.8%	11.4%	11.3%	6.5%	5.4%	5.6%	8.7%	5.1%	12.4%

4.3. Fatigue Life Prediction

According to the elastic/plastic finite element analysis under the simulated load, the stress and strain response could be obtained to calculate fatigue life of welded A-type frame. The cyclic material properties were based on Table 3, and the linear cumulative damage rule was still used in this estimation. Taking the mean stress into account, the Smith-Waston-Topper (SWT) correction method was utilized in the MSC software. Fatigue was considered to have good precision in high plastic strain field. Then, the lifetime contour of welded A-type frame was acquired, as shown in Figure 23. The minimum fatigue life of this welded A-type frame was 11,203 cycles (about 24 cycles a day) and located at the bottom corner between front plates and back plates. Visual inspections of the welded A-type frame revealed the crack (seen in Figure 2) at the right bottom weld toe after the truck ran for

13 months at the downhill and turning condition, and the simulated results was in good agreement with the tested ones. According to the calculated results, the fatigue life of welded A-type frame has to be increased, because its current lifetime was not in compliance with engineering requirements.

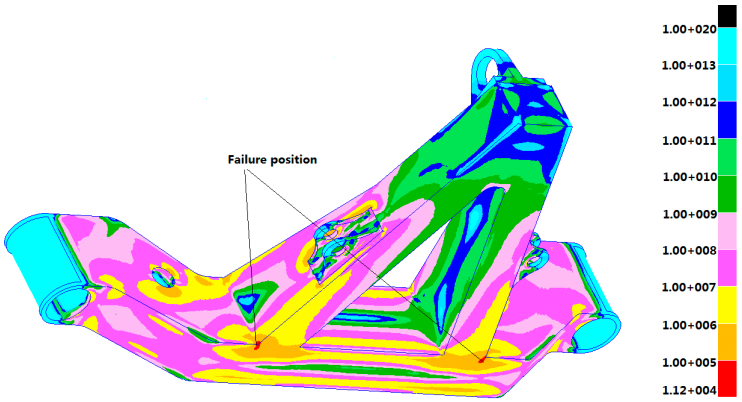

Figure 23. Fatigue life contour of welded A-type frame (cycles).

5. Lifetime and Weight Co-Optimization

5.1. Multi-Objective Optimization Function

The lifetime of an engineering structure is related to geometry dimension, material properties, and bearing load. However, there is permissible deviation for the dimensions of structure, and the manufacturing process would also result in the uncertainty of geometry. The material properties could change because of different forming conditions and artificial operating. The dynamic loads are bound to keep varying in service time. Therefore, those uncertainty variables of geometry dimensions, material properties, and bearing loads were all taken into account in lifetime and weight co-optimization in this paper. The thickness of front and back plates in this frame would vary in ranges, as shown in Figure 19, as well as the cyclic material parameters σ'_f, ε'_f, b and c. The four main bearing loads at four connection sites (marked as A1, A2, A3, and A4 in Figure 19) were also defined to be variables. Then, the multi-objectives optimization function was described as:

$$\begin{gathered} \min \quad Mass(x0, x1, x2) \\ \max \quad Life(x0, x1, x2, x3, x4, x5, x6, x7, x8, x9, x10) \\ s.t. \quad Life \geq 2.0e5; mass \leq 4.0e3kg; 0 \leq x0 \leq 100; 15 \leq x1 \leq 25;\ 24 \leq x2 \leq 40; \\ 872.6 \leq x3 \leq 1454.3; -0.1554 \leq x4 \leq -0.0932; 0.119 \leq x5 \leq 0.198; \\ -0.3269 \leq x6 \leq -0.1961; -2.50e5 \leq x7 \leq -1.50e5; 7.88e4 \leq x8 \leq 1.31e5; \\ 7.95e4 \leq x9 \leq 1.32e5; -5.01e5 \leq x10 \leq -3.01e5; \end{gathered}$$

where *Mass* function stood for the optimization objective of weight and $Life$ function stood for the optimization objective of lifetime. The distance of weld metal away from the back plates was defined as $x0$, marked as d in Figure 19. The weighting coefficient of two optimization objectives was assigned to be 0.3 and 0.7 in the light of engineering experience. The geometry variables $x1$ and $x2$ were thickness of front and back plates. The cyclic material parameters $x3$, $x5$ were the fatigue strength coefficient and the fatigue ductility coefficient, and the parameters $x4$, $x6$ the fatigue strength exponent and the fatigue ductility exponent, respectively. The bearing loads $x7$, $x8$, $x9$, and $x10$ were the peak vertical force along Y direction at connection site A1, the peak lateral force along X direction at connection site A2–A4, respectively.

In order to build the relationship between objectives and variables, the Latin hypercube sampling method was first used to get the 50 sample points, listed in Table 5.

Table 5. Sample points from the Latin hypercube method.

Run Counter	*x*0 (mm)	*x*1 (mm)	*x*2 (mm)	*x*3 (MPa)	*x*4	*x*5	*x*6	*x*7 ($\times 10^5$N)	*x*8 ($\times 10^5$N)	*x*9 ($\times 10^5$N)	*x*10 ($\times 10^5$N)
1	0	18	27	1311.8	−0.0995	0.119	−0.2788	−1.89	0.86	1.01	−3.83
2	10	22	31	1098.1	−0.1287	0.169	−0.3002	−1.96	1.02	0.88	−3.66
3	20	16	29	1430.5	−0.1313	0.197	−0.2228	−1.65	1.07	0.81	−5.01
4	30	24	35	1003.1	−0.1135	0.168	−0.2575	−1.85	1.18	1.14	−4.07
5	40	19	36	1193.1	−0.1376	0.125	−0.3242	−1.87	0.99	0.95	−4.43
6	50	15	26	1169.3	−0.1439	0.132	−0.2067	−2.04	1.11	1.31	−4.03
7	60	21	37	1406.8	−0.1414	0.187	−0.2362	−1.81	0.92	1.01	−4.28
8	70	20	34	920.0	−0.0982	0.189	−0.2815	−2.25	1.22	1.03	−4.97
9	80	17	35	1371.2	−0.1351	0.155	−0.2468	−2.49	0.83	1.06	−3.29
...		...	...	...	...	...	...	...	...	...	...
50	100	23	38	1121.85	−0.1300	0.164	−0.2175	−2.22	0.84	0.84	−4.93

When the optimization design variables were determined, the corresponding response values could be obtained from the finite element analysis. Then, their approximation relationship could be constructed to start the multi-objectives optimization. In this paper, the Kriging approximation model was chosen to describe their mathematical links, while the NSGA-II was used to search for the optimal solution in this optimization problem. These two methods are described in my previous works [22,23]. The whole optimization process is shown in Figure 24.

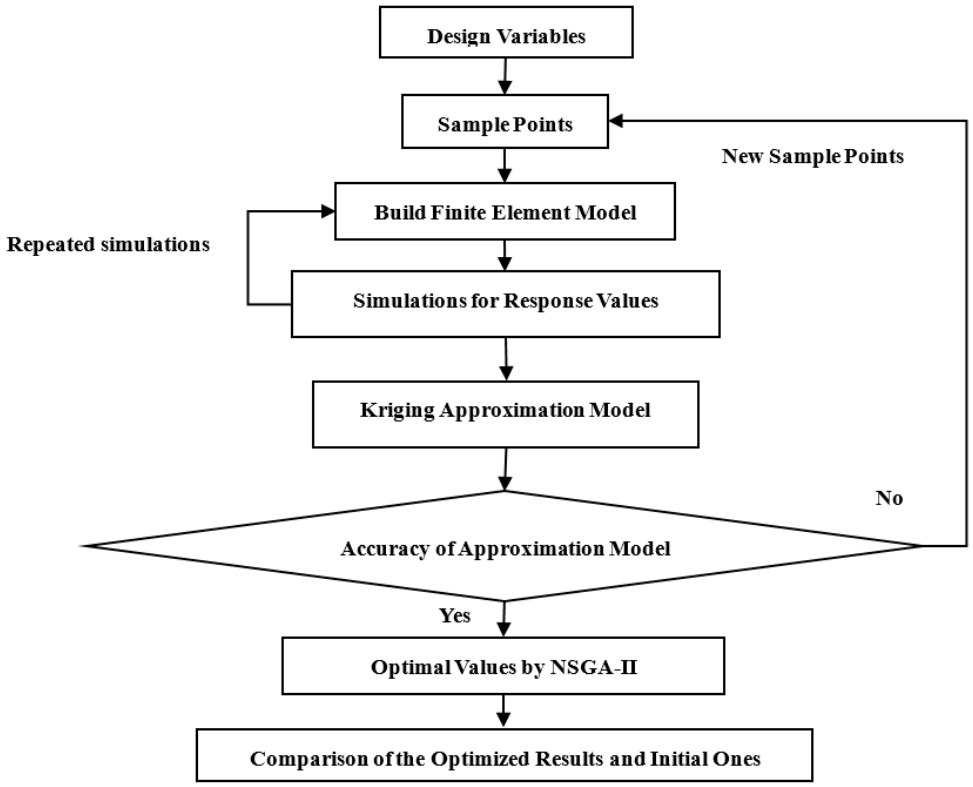

Figure 24. Chart of optimization process.

5.2. Approximation Model

The Kriging approximation model could take the place of the finite element model to describe the relationship between design variables and optimization objectives, which was explained in my previous publications [22,23]. In this paper, the other 10 sample points obtained from Latin hypercube sampling method were used to testify the accuracy of the approximation model, shown in Figure 25. If the coefficient of determination R is closer to 1.0, it means the fitting model has the best accuracy.

The Kriging approximation model for both weight and lifetime met the accuracy requirement for this engineering optimization problem.

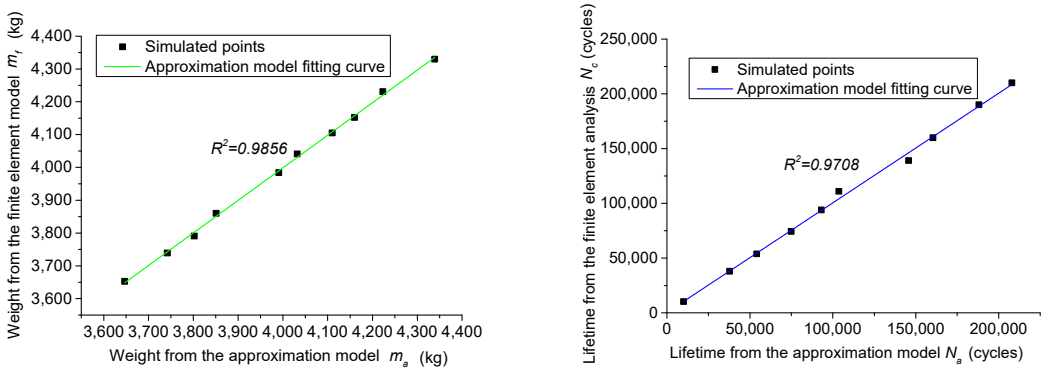

Figure 25. Accuracy of approximation model: (**a**) weight of welded A-type frame; (**b**) fatigue life of welded A-type frame.

5.3. Optimization Results

In this paper, the NSGA-II was selected to conduct this multi-objectives optimization. The Pareto frontiers were obtained after running 27 min and 2450 iterations, from which a compromised solution was treated as the optimal result with comprehensive consideration of two conflicting optimization objectives, listed in Table 6. The distance of weld metal away from the back plates increased to 40 mm and the thickness of front plates increased to 24mm as well, which could weaken the stress level at stress concentration areas, shown in Figure 26. The maximum stress from the optimized structure decreased to 285 MPa. According to the optimized results, it was beneficial to extend fatigue life of this welded A-type frame when four absolute cyclic material parameters increased and four loads at connection sites were decreased. It could be deduced that better welding quality would improve the fatigue performance of welded joints and lower speed could result in small load. As such, enhancing the weldment quality and limiting drive speed for mining truck are able to ensure fatigue performances of welded A-type frame. As shown in Table 6, the reduction of the thickness of back plates mainly contributed to lightweight of this frame. The minimum fatigue life of welded A-type frame went up to 2.40×10^5 cycles, and its weight was reduced by 8.2%, which was also achieved by reducing the thickness of back plates. The simulated fatigue life contour for the optimal solution is displayed in Figure 27. The minimum fatigue life was close to the calculated one (around 2.33×10^5 cycles) obtained from the approximation model and satisfied with the design requirement.

Table 6. Comparison of the initial and optimized results.

	*x*0 (mm)	*x*1 (mm)	*x*2 (mm)	*x*3 (MPa)	*x*4	*x*5	*x*6	*x*7 ($\times 10^5$N)	*x*8 ($\times 10^5$N)	*x*9 ($\times 10^5$N)	*x*10 ($\times 10^5$N)	Lifetime (Cycles)	Weight (kg)
initial	0	20	32	1163.4	−0.1243	0.159	−0.2615	−2.03	1.05	1.06	4.01	11203	4135
optimized	40	24	27	1381.1	−0.1393	0.189	−0.2956	1.84	0.89	0.93	−3.32	240180	3797

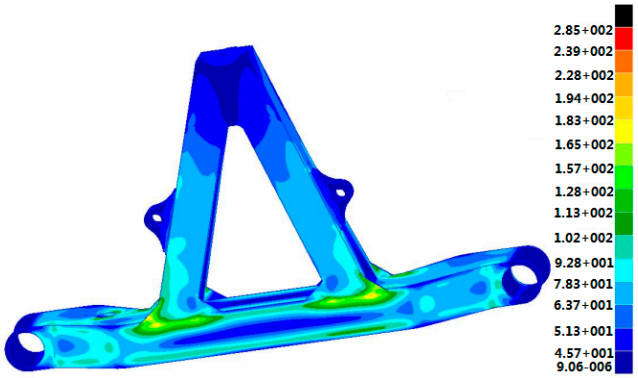

Figure 26. Stress contour of optimized welded A-type frame (MPa).

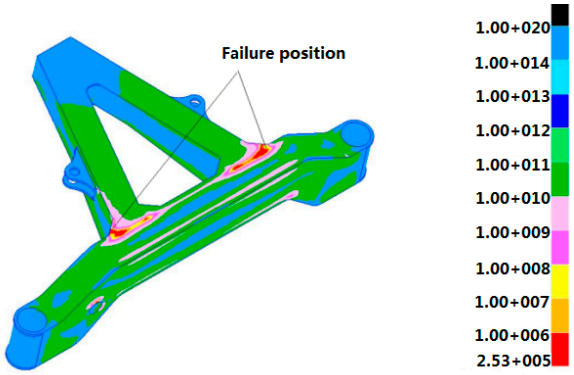

Figure 27. Fatigue life contour of optimized welded A-type frame (cycles).

6. Conclusions

This paper firstly aimed to analyze the fatigue failure of welded A-type frame based on experiment works and simulation method. The monotonic tensile properties for the weld metal and base metal were both studied and found to be very similar. The fatigue test of the welded joints was implemented to obtain cyclic properties used for the lifetime estimation. The multi-body dynamic model was built to get load history for the welded A-type frame, and its accuracy was validated with the experimental results. The finite element model of this frame was generated to observe the stress distribution, and its accuracy was also verified by comparing the test results with the simulated stresses. The fatigue life of welded A-type frame was predicted and found to be far less than the design requirement, while its predicted failure position was in good agreement with experimental observations.

Then, considering the multi-uncertainties in geometry dimension, material properties, and bearing load, a co-optimization method for increasing lifetime and lightweight was presented, based on the Kriging approximation model. The multi-objectives optimization function was built. The 50 sample points were obtained by Latin hypercube sampling method, and their responses were calculated by the elastic/plastic finite element analysis. The constructed Kriging approximation model was verified with other 10 sample points, and its accuracy was found to be satisfactory. The NSGA-II was utilized to optimize this multi-objective optimization problem. The distance of weld metal away from the back plates and the thickness of front plates and four absolute cyclic material parameters increased, while the thickness of back plates and four loads at connection sites decreased. Finally, the lifetime of this welded A-type frame increased to 2.40e5 cycles and its weight decreased by 8.2%.

Author Contributions: Conceptualization, C.M. and F.B.; Methodology, C.M.; Software, W.L.; Validation, W.L., X.X. and Z.G.; Formal analysis, C.M.; Investigation, C.M.; Resources, Z.G.; Data Curation, X.X.; Writing—Original Draft Preparation, C.M.; Writing—Review & Editing, F.B.; Visualization, H.J; Supervision, H.J.; Project Administration, C.M.; Funding Acquisition, C.M. and H.J.

Funding: This research was funded by [Natural Science Foundation of Hunan Province] grant number [2017JJ3059 and 2018JJ4060], and [Postdoctoral Science Foundation] grant number [2017M622569], and [State Key Laboratory of Advanced Design and Manufacturing for Vehicle Body] grant number [31715012].

Acknowledgments: The authors gratefully acknowledge the support of the Hunan Province Natural Science Foundation (Grant No.:2017JJ3059 and 2018JJ4060), China Postdoctoral Science Foundation (Grant No.:2017M622569), and Open Foundation of State Key Laboratory of Advanced Design and Manufacturing for Vehicle Body (Grant No.:31715012).

Conflicts of Interest: The authors declare no conflict of interest. The funders had no role in the design of the study; in the collection, analyses, or interpretation of data; in the writing of the manuscript, and in the decision to publish the results.

References

1. Gu, Z.; Mi, C.; Wang, Y.; Jang, J. A-type frame fatigue life estimation of a mining dump truck based on modal stress recovery method. *Eng. Fail. Anal.* **2012**, *26*, 89–99. [CrossRef]
2. Wannenburg, J.; Heyns, P.S.; Raath, A.D. Application of a fatigue equivalent static load methodology for the numerical durability assessment of heavy vehicle structures. *Int. J. Fatigue* **2009**, *31*, 1541–1549. [CrossRef]
3. Tovo, R.; Livieri, P. A numerical approach to fatigue assessment of spot weld joints. *Fatigue Fract. Eng. Mater. Struct.* **2010**, *34*, 32–45. [CrossRef]
4. Kang, H.T. Fatigue prediction of spot welded joints using equivalent structural stress. *Mater. Des.* **2007**, *28*, 837–843. [CrossRef]
5. Varvani-Farahani, A.; Kodric, T.; Ghahramani, A. A method of fatigue prediction in notched and un-notched components. *J. Mater. Process. Technol.* **2005**, *169*, 94–102. [CrossRef]
6. Wang, P.C.; Ewing, K.W. Fracture mechanics analysis of fatigue resistance of spot welded coach-peel joints. *Fatigue Fract. Eng. Mater. Struct.* **1991**, *14*, 915–930. [CrossRef]
7. Ayala-Uraga, E.; Moan, T. Fatigue reliability based assessment of welded joints applying consistent fracture mechanics formulations. *Int. J. Fatigue* **2007**, *29*, 444–456. [CrossRef]
8. Fischer, C.; Fricke, W.; Rizzo, C.M. Review of the fatigue strength of welded joints based on the notch stress intensity factor and SED approaches. *Int. J. Fatigue* **2016**, *84*, 59–66. [CrossRef]
9. Jahed, H.; Varvani Farahani, A.; Noban, M.; Khalaji, I. An energy based fatigue life assessment model for various metallic materials under proportional and non-proportional loading conditions. *Int. J. Fatigue* **2007**, *29*, 647–655. [CrossRef]
10. Jiang, C.; Liu, Z.C.; Wang, X.G.; Zhang, Z.; Long, X.Y. A structural stress-based critical plane method for multi-axial fatigue life estimation in welded joints. *Fatigue Fract. Eng. Mater. Struct.* **2016**, *39*, 372–383. [CrossRef]
11. Michael, K. Improvements in the fatigue assessment of large welded structure using the nominal stress approach. *SAE* **2012**, *1*, 1910.
12. Shao, Y.; Liu, J.; Mechefske, C.K. Drive axle housing failure analysis of a mining dump truck based on the load spectrum. *Eng. Fail. Anal.* **2011**, *18*, 1049–1057. [CrossRef]
13. Mi, C.; Gu, Z.; Yang, Q.; Nie, D. Frame fatigue life assessment of a mining dump truck based on finite element method and multi-body dynamic analysis. *Eng. Fail. Anal.* **2012**, *23*, 18–26. [CrossRef]
14. Yang, Q.; Gu, Z.; Mi, C. An analysis on the fatigue life of frame in SF33900 mining dump truck. *Autom. Eng.* **2012**, *23*, 1015–1019.
15. Gu, Z.; Mi, C.; Ding, Z.; Zhang, Y.; Liu, S.; Nie, D. An energy-based fatigue life prediction of a mining truck welded frame. *J. Mech. Sci. Technol.* **2016**, *30*, 3615–3624. [CrossRef]
16. Berto, F.; Campagnolo, A.; Chebat, F.; Cincera, M.; Santini, M. Fatigue strength of steel rollers with failure occurring at the weld root based on the local strain energy values: Modelling and fatigue assessment. *Int. J. Fatigue* **2016**, *82*, 643–657. [CrossRef]
17. Berto, F.; Vinogradov, A.; Filippi, S. Application of the strain energy density approach in comparing different design solutions for improving the fatigue strength of load carrying shear welded joints. *Int. J. Fatigue* **2017**, *101*, 371–384. [CrossRef]
18. Fang, J.; Gao, Y.; Sun, G.; Xu, C.; Li, Q. Multi-objective robust design optimization of fatigue life for a truck cab. *Reliab. Eng. Syst. Saf.* **2015**, *135*, 1–8. [CrossRef]

19. Aoues, Y.; Pagnacco, E.; Lemosse, D.; Khalij, L. Reliability-based design optimization applied to structures submitted to random fatigue loads. *Struct. Mulidisc. Optim.* **2017**, *55*, 1471–1482. [CrossRef]
20. Hu, W.; Choi, K.K.; Cho, H. Reliability-based design optimization of wind turbine blades for fatigue life under dynamic wind load uncertainty. *Struct. Mulidisc. Optim.* **2016**, *54*, 953–970. [CrossRef]
21. Gao, Y.; Liu, Q.; Wang, Y.; Zhao, W. Lightweight design with weld fatigue constraints for a three-axle bogie frame using sequential approximation optimization method. *Int. J. Veh. Des.* **2017**, *73*, 3–19. [CrossRef]
22. Mi, C.; Gu, Z.; Zhang, Y.; Liu, S.; Zhang, S.; Nie, D. Frame weight and anti-fatigue co-optimization of a mining dump truck based on Kriging approximation model. *Eng. Fail. Anal.* **2016**, *66*, 99–109. [CrossRef]
23. Mi, C.; Gu, Z.; Jian, H. Anti-fatigue and lightweight design for frame structures of electric wheel dump truck. *China Mech. Eng.* **2017**, *28*, 2455–2462.